

[Am]Mn(H₂POO)₃: A New Family of Hybrid Perovskites Based on the Hypophosphite Ligand

Yue Wu,^{†,§} Sammy Shaker,^{†,§} Federico Brivio,^{†,§} Ramaswamy Murugavel,^{‡,§} Paul D. Bristowe,^{*,†} and Anthony K. Cheetham^{*,†}

[†]Department of Materials Science and Metallurgy, University of Cambridge, 27 Charles Babbage Road, Cambridge CB3 0FS, United Kingdom

[‡]Department of Chemistry, Indian Institute of Technology Bombay, Powai, Mumbai-400076, India

S Supporting Information

ABSTRACT: A family of five hybrid ABX₃ perovskites has been synthesized using hypophosphite (H₂POO)[−] as the X-site ion. These compounds adopt the general formula [Am]Mn(H₂POO)₃, where Am = guanidinium (GUA), formamidinium (FA), imidazolium, triazolium, and dabconium. We explore the diverse structural and phase transition behavior of these materials through single-crystal diffraction measurements and demonstrate contrasting magnetism in two of the phases, Am = GUA and FA, that arises from structural distortions. The results show that hypophosphite perovskites offer a promising platform for generating new functional materials.

Since the discovery of the first perovskite, CaTiO₃, the ABX₃ perovskite topology has recurred frequently in materials chemistry and condensed matter physics as a system that is very tolerant to substitution. In recent years, the replacement of the monatomic A or X site ions with molecular ions has given rise to a large family of hybrid (organic–inorganic) perovskites, many of which display exceptional functional properties beyond those of classical perovskites.¹ A key example is the alkylammonium lead halide family, which has revolutionized the field of photovoltaics.² In this family, the anisotropic dynamics of alkylammonium ion play an important role in controlling optoelectronic properties.³ More generally, the anisotropy and greater chemical diversity of possible A- and X-site molecular ions in hybrid perovskites gives the potential for more types of ordering and symmetry-breaking, allowing for more subtle tuning of structure and hence function, compared to inorganic systems.

When both A and X site ions are molecular, a large structural diversity becomes accessible, giving rise to further functionality. The alkylammonium metal(II) formate family^{4,5} is the most extensive and contains ferroelectric^{6–8} and multiferroic members.^{9–11} Known hybrid perovskite families with molecular X-sites include azides,¹² dicyanamides,¹³ dicyanometallates,¹⁴ cyanides,¹⁵ thiocyanates,¹⁶ and borohydrides.¹⁷ Herein we report the synthesis and characterization of a new family of hybrid perovskites where X = (H₂POO)[−] (hypophosphite). This new linker has the advantages of being cheap, nontoxic, and earth-abundant. We have previously noted the structural and functional similarities of hypophosphite to formate (Figure 1) that make it a promising platform for new perovskites.¹⁸ We

also note the existence of V(H₂PO₂)₃, which has the parent *reo* topology.¹⁹

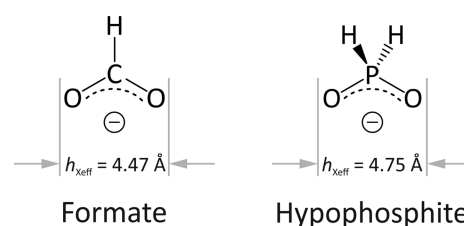


Figure 1. Comparison of formate and hypophosphite.

Using the Goldschmidt tolerance factor modified for hybrid perovskites,^{20,21} we predicted compositions likely to adopt the perovskite structure when X = hypophosphite. We then succeeded in synthesizing perovskites with five different A-site amine cations: guanidinium (GUA), formamidinium (FA), imidazolium (IM), triazolium (TRZ), and 1,4-diazabicyclo[2.2.2]octane-1,4-diium or “DABCONium” (DAB) (see Supporting Information for details). All of the new phases have tolerance factors in the range 0.86–0.91 (Table 1). In a typical synthesis, manganese carbonate (1 equiv) was dissolved in excess aqueous hypophosphorous acid solution (50% w/w; 6 equiv). The alkylamine or alkylammonium salt (1 equiv) was

Table 1. Tolerance Factors (α) and Distortion Factors (δ) for Hypophosphite and Formate (bolded) Perovskites

compound	α	space group	δ
[GUA]Mn(H ₂ POO) ₃	0.91	<i>P</i> $\bar{1}$	0.6%
[GUA]Mn(H ₂ POO) ₃	0.91	<i>I</i> 2/ <i>m</i>	0.5%
[GUA]Mn(HCOO)₃	0.96	<i>P</i>nna	0.3%
[FA]Mn(H ₂ POO) ₃ (RT)	0.86	<i>C</i> 2/ <i>c</i>	10.6%
[FA]Mn(H ₂ POO) ₃ (115 K)	0.86	<i>P</i> 2 ₁ / <i>c</i>	11.1%
[FA]Mn(HCOO)₃	0.90	<i>C</i>2/<i>c</i>	0.9%
[IM]Mn(H ₂ POO) ₃	0.87	<i>P</i> 2 ₁ / <i>c</i>	1.9%
[IM]Mn(HCOO)₃	0.91	<i>P</i>2₁/<i>n</i>	0.2%
[TRZ]Mn(H ₂ POO) ₃	0.87	<i>P</i> 2 ₁ / <i>c</i>	5.4%
[DAB]Mn ₂ (H ₂ POO) ₆ (RT)	0.90	<i>R</i> $\bar{3}$	1.7%
[DAB]Mn ₂ (H ₂ POO) ₆ (120 K)	0.90	<i>P</i> $\bar{1}$	1.6%

Received: September 3, 2017

Published: October 25, 2017

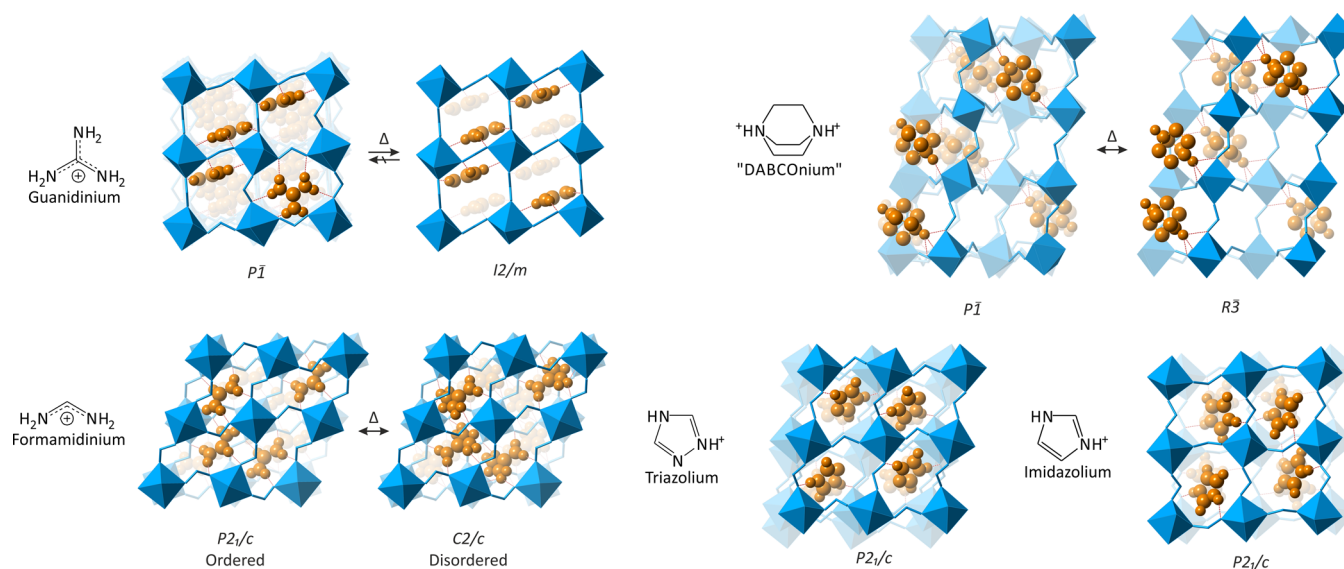


Figure 2. Structural diagrams of $[\text{Am}]\text{Mn}(\text{H}_2\text{POO})_3$ phases, including phase transitions. The $\text{Mn}-(\text{H}_2\text{POO})$ frameworks are shown in blue with $\text{Mn}-\text{O}_6$ octahedra drawn. A-site cations are shown in orange with space-filling representation. All structures are viewed down one axis of the perovskite cage, except $[\text{DAB}]\text{Mn}(\text{H}_2\text{POO})_3$ which is viewed down a face diagonal to clarify the A-site ordering.

then added and stirred until dissolved. Using these solutions, crystals were obtained using slow evaporation at 50 °C or through vial-in-vial diffusion (see SI for full synthetic details).

Figure 2 shows the structures of the five $[\text{Am}]\text{Mn}(\text{H}_2\text{POO})_3$ perovskites. GUA, FA, IM, and TRZ form conventional ABX_3 perovskites, whereas DAB forms an ordered A-site double perovskite of the form $\text{A}\varnothing\text{M}_2\text{X}_6$ ($\varnothing = \text{vacancy}$), with DAB^{2+} cations occupying 50% of the perovskite cages. Mn formate perovskites containing GUA,⁵ IM,²² and FA²³ are known, so hypophosphite might be expected to form structurally similar phases. However, hypophosphite appears to be significantly more flexible and our results show that the hypophosphite perovskites display significantly greater cage distortions, giving rise to additional symmetry-breaking elements in the form of classically forbidden Glazer tilts²⁴ or and columnar shifts²⁵ (i.e., shearing of whole columns or sheets of octahedra).

To highlight the difference between the formate and hypophosphite perovskites, we introduce a “distortion factor”, δ , (eq 1), which compares the actual volume of a single perovskite cage (V_{real}) to that of an idealized cubic cage with the average crystallographic $\text{M}-\text{M}'$ distance (V_{ideal}) in that phase, to show how far that structure departs from the cubic aristotype. Table 1 clearly shows that while δ_{formate} reaches a maximum of 1%, $\delta_{\text{hypophosphite}}$ is considerably higher in several cases.

$$\delta = \left[\frac{V_{\text{ideal}}}{V_{\text{real}}} - 1 \right] \times 100\% \quad (1)$$

$[\text{GUA}]\text{Mn}(\text{H}_2\text{POO})_3$ forms two polymorphs at room temperature: triclinic $P\bar{1}$ ($V_{\text{RT}} = 1111.4 \text{ \AA}^3$) and monoclinic $I2/m$ ($V_{\text{RT}} = 1121.1 \text{ \AA}^3$). Both structures are fully ordered, with all six GUA N–H hydrogens H-bonding to the inorganic framework. In the triclinic form, the GUA cations order parallel to two perpendicular planes, whereas in the monoclinic modification the cations all lie parallel to one plane (Figure 2). Single-crystal X-ray diffraction shows an irreversible single-crystal-to-single-crystal transformation of the triclinic to the monoclinic form on heating to 400 K, indicating that the latter is the high temperature modification. It is possible that the

triclinic phase is the kinetic phase and converts to the monoclinic phase upon thermal disruption of the GUA H-bonding, or that the less dense monoclinic phase is stabilized by vibrational entropy at high temperatures, as has been observed in other perovskite-related ABX_3 polymorphs.²⁶

$[\text{FA}]\text{Mn}(\text{H}_2\text{POO})_3$ crystallizes in $C2/c$ at room temperature with FA disordered over two positions. It undergoes a reversible order–disorder phase transition at ca. 175 K, with FA ordering in the space group $P2_1/c$. This behavior suggests ferroelectric phases could potentially be generated through further chemical tuning. The N–H hydrogens of both forms are fully hydrogen bonded to the framework. This phase has very pronounced layer shearing in one direction, resulting in a distortion parameter, δ , over ten times higher than the corresponding formate phase. This arises from the framework shearing in order to accommodate the highly anisotropic, rod-like FA molecules, highlighting the ability of the $\text{Mn}-(\text{H}_2\text{POO})$ framework to more readily adapt to differences in the shape of the A-site cation compared to the formates.

$[\text{IM}]\text{Mn}(\text{H}_2\text{POO})_3$ and $[\text{TRZ}]\text{Mn}(\text{H}_2\text{POO})_3$ both crystallize in $P2_1/c$ and have fully ordered cations with no phase transitions in the 120–450 K temperature range. As both phases hydrogen bond through the N–H hydrogens at the 1 and 4 positions of the heterocycle, similar structures would be expected. However, $[\text{TRZ}]\text{Mn}(\text{H}_2\text{POO})_3$ is significantly more distorted ($\delta_{\text{TRZ}} = 5.4\%$, $\delta_{\text{IM}} = 1.9\%$), perhaps due to the higher polarity of TRZ.

$[\text{DAB}]\text{Mn}_2(\text{H}_2\text{POO})_6$ forms an ordered $\text{DAB}^{2+}/\text{vacancy}$ A-site double perovskite with rhombohedral symmetry. To our knowledge, the only other A-site vacancy double perovskites are the Ln A-site oxides.²⁷ This perovskite does not follow any known AA' ordering patterns, such as rock-salt, columnar, or layered normal to the perovskite $[100]$ axes.²⁸ Instead, it adopts an unprecedented pattern of alternating double layers of DAB and vacancies normal to the perovskite cage body diagonal. This ordering reflects the 3-fold symmetry of both DAB and perovskite around the body diagonal, with the hypophosphite ligands pointing into the vacant cages to accommodate the bulky DAB in the others. Each N–H hydrogen is within

hydrogen bonding distance to three equidistant oxygens of an Mn–O₆ octahedral face. The formation of [DAB]-Mn₂(H₂POO)₆ appears to be entropically stabilized as it forms on overnight heating of the reaction mixture in air at ca. 50 °C. However, it is metastable at room temperature, degrading to binary Mn hypophosphites over several days. The process is reversible. At low temperatures, [DAB]-Mn₂(H₂POO)₆ undergoes a reversible symmetry lowering transition to a triclinic *P* $\bar{1}$ phase (measured at 120 K), though the refinement of the triclinic phase is rather modest.

All of the bulk samples contain impurities, but reasonably pure samples of two phases, [GUA]Mn(H₂POO)₃ and [FA]Mn(H₂POO)₃, could be obtained through manual separation of single crystals. PXRD data of these two samples showed good purity for the GUA phase and low levels of impurities for the FA phase (see SI for refinements against the PXRD data). Magnetic susceptibility data were collected for these two phases. The results (Figure 3) show that the GUA

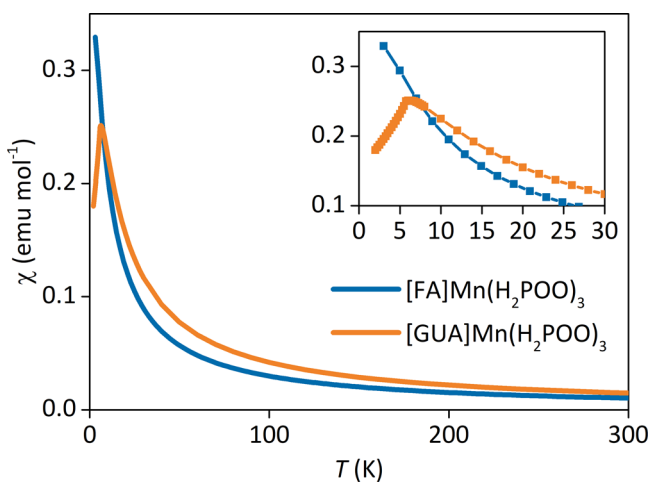


Figure 3. Zero field cooled magnetic susceptibilities of [FA]Mn(H₂POO)₃ (blue) and [GUA]Mn(H₂POO)₃ (orange). Zoom inset.

phase orders antiferromagnetically at low temperatures, with a Néel temperature of 6.5 K; this is very similar to that of [GUA]Mn(HCOO)₃, which is 8.8 K.⁵ In the paramagnetic region, it follows the Curie–Weiss law, with a negative Weiss constant of –9.9 K and an effective magnetic moment of 6.1 μ_B (see SI for further details). The expected value of the spin for a high spin *d*⁵ ion is 5.92 μ_B . In the case of the FA phase, there is no magnetic ordering but the system follows the Curie–Weiss law with a Weiss constant of –5.8 K and an effective magnetic moment of 5.0 μ_B (see SI). We attribute this unusually low moment to the presence of diamagnetic impurities. This behavior is in contrast to [FA]Mn(HCOO)₃, which is a weak ferromagnet with *T*_c = 8.0 K.²³ In order to probe the origin of the different behaviors, we performed density functional calculations, as described below.

Spin-polarized DFT simulations²⁹ predict that the uniform metal–ligand environments in [GUA]Mn(H₂POO)₃ should mediate antiferromagnetic (AFM) exchange, as observed in our own work and in other Mn hypophosphites.¹⁸ However, whereas the most uniform of the three metal–ligand–metal environments in [FA]Mn(H₂POO)₃ shows both similar geometry and magnetic behavior to [GUA]Mn(H₂POO)₃, the other two metal environments are highly distorted (Figure 4). In simulation, this results in a higher-energy layered AFM

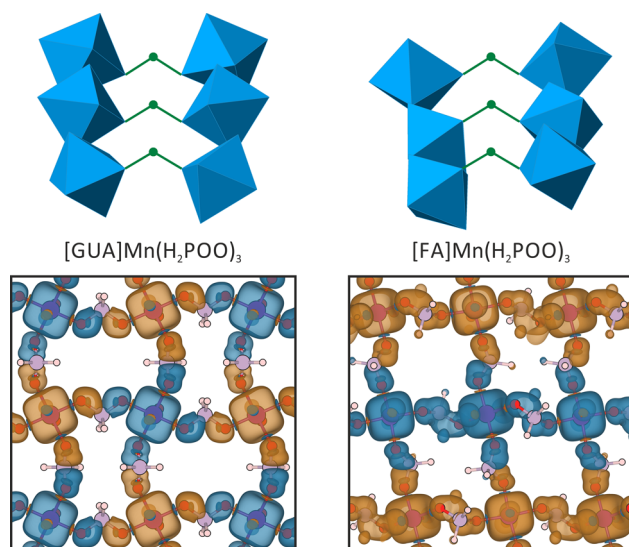


Figure 4. (Above) Comparison of the symmetry-unique Mn–H₂POO bonding geometries in [GUA]Mn(H₂POO)₃ and [FA]Mn(H₂POO)₃ and (below) electronic spin density isosurfaces for each phase obtained from spin-polarized density functional theory calculations (opposing spins shown in blue and orange).

state, which is consistent with the negative Weiss constant from the Curie–Weiss fit but probably accounts for the lack of observed ordering (details in SI). Comparative electronic spin density isosurfaces for the two phases are shown in Figure 4.

In summary, we have synthesized and characterized a family of X = (H₂POO)[–] hybrid perovskites with five different A-site amine cations. The rich structural diversity, phase transitions, and magnetic behavior of these phases demonstrate that hypophosphite is a promising candidate for generating chemically tunable functional perovskite materials, such as ferroelectrics and multiferroics. By analogy with other perovskite X-site ions such as formate and azide, it is clear this work could lead to a large family of new hybrid perovskites. The use of other A- and B-site cations presents excellent opportunities for future work, along with solid solution studies and the formation of other double perovskites. X-site solid solutions and ordered mixtures are particularly rare for perovskites, so the similarity in size between formate and hypophosphite presents this as an exciting direction for additional research.

■ ASSOCIATED CONTENT

Supporting Information

The Supporting Information is available free of charge on the ACS Publications website at DOI: 10.1021/jacs.7b09417.

Further details of experimental and computational methods, crystallography, and tolerance factor calculations (PDF)

Data for CCDC 1582415 [FA]Mn(H₂POO)₃ (115 K) (CIF)

Data for CCDC 1582416 [FA]Mn(H₂POO)₃ (RT) (CIF)

Data for CCDC 1582418 [GUA]Mn(H₂POO)₃ (monoclinic, RT) (CIF)

Data for CCDC 1582419 [GUA]Mn(H₂POO)₃ (triclinic, RT) (CIF)

Data for CCDC 1582417 [IM]Mn(H₂POO)₃ (RT) (CIF)

Data for CCDC 1582421 [TRZ]Mn(H₂POO)₃ (RT) (CIF)

Data for CCDC 1582420 [DAB]Mn(H₂POO)₃ (120 K) (CIF)

Data for CCDC 1582414 [DAB]Mn(H₂POO)₃ (RT) (CIF)

AUTHOR INFORMATION

Corresponding Authors

*akc30@cam.ac.uk

*pdb1000@cam.ac.uk

ORCID

Yue Wu: [0000-0003-2874-8267](https://orcid.org/0000-0003-2874-8267)

Federico Brivio: [0000-0001-6807-4872](https://orcid.org/0000-0001-6807-4872)

Ramaswamy Murugavel: [0000-0002-1816-3225](https://orcid.org/0000-0002-1816-3225)

Paul D. Bristowe: [0000-0002-3153-1387](https://orcid.org/0000-0002-3153-1387)

Anthony K. Cheetham: [0000-0003-1518-4845](https://orcid.org/0000-0003-1518-4845)

Author Contributions

[§]These authors contributed equally.

Notes

The authors declare no competing financial interest.

ACKNOWLEDGMENTS

Y.W., F.B., and A.K.C. gratefully thank the Ras Al Khaimah Center for Advanced Materials for financial support. S.S. gratefully thanks the Winston Churchill Foundation of the USA for financial support. R.M. thanks SERB, New Delhi for a JC Bose Fellowship. DFT calculations were performed at the Cambridge HPCS and the UK National Supercomputing Service, ARCHER. Access to the latter was obtained via the MCC consortium and funded by EPSRC under Grant No. EP/L000202/1. Magnetic measurements were carried out using the Advanced Materials Characterization Suite, funded by EPSRC Strategic Equipment Grant EP/M000524/1. We thank Dr. M. J. Cliffe and Dr M. W. Gaultois for helpful discussions, and Dr Cliffe for the use of his SQUID TIME code for fitting and plotting magnetic data.

REFERENCES

- (1) Li, W.; Wang, Z.; Deschler, F.; Gao, S.; Friend, R. H.; Cheetham, A. K. *Nat. Rev. Mater.* **2017**, *2* (3), 16099.
- (2) Saparov, B.; Mitzi, D. B. *Chem. Rev.* **2016**, *116* (7), 4558.
- (3) Lee, J.-H.; Bristowe, N. C.; Bristowe, P. D.; Cheetham, A. K. *Chem. Commun.* **2015**, *51* (29), 6434.
- (4) Wang, X. Y.; Gan, L.; Zhang, S. W.; Gao, S. *Inorg. Chem.* **2004**, *43* (15), 4615.
- (5) Hu, K. L.; Kurmoo, M.; Wang, Z.; Gao, S. *Chem. - Eur. J.* **2009**, *15* (44), 12050.
- (6) Chen, S.; Shang, R.; Wang, B. W.; Wang, Z. M.; Gao, S. *Angew. Chem., Int. Ed.* **2015**, *54* (38), 11093.
- (7) Chen, S.; Shang, R.; Hu, K.-L.; Wang, Z.-M.; Gao, S. *Inorg. Chem. Front.* **2014**, *1*, 83.
- (8) Jain, P.; Dalal, N. S.; Toby, B. H.; Kroto, H. W.; Cheetham, A. K. *J. Am. Chem. Soc.* **2008**, *130* (32), 10450.
- (9) Jain, P.; Ramachandran, V.; Clark, R. J.; Zhou, H. D.; Toby, B. H.; Dalal, N. S.; Kroto, H. W.; Cheetham, A. K. *J. Am. Chem. Soc.* **2009**, *131* (38), 13625.
- (10) Xu, G.-C.; Zhang, W.; Ma, X.-M.; Chen, Y.-H.; Zhang, L.; Cai, H.-L.; Wang, Z.-M.; Xiong, R.-G.; Gao, S. *J. Am. Chem. Soc.* **2011**, *133* (38), 14948.
- (11) Maćzka, M.; Gagor, A.; Ptak, M.; Paraguassu, W.; da Silva, T. A.; Sieradzki, A.; Pikul, A. *Chem. Mater.* **2017**, *29* (5), 2264.

(12) Mautner, F. A.; Krischner, H. Z. *Kristallogr. - Cryst. Mater.* **1986**, *175* (1–4), 105.

(13) Tong, M.-L.; Ru, J.; Wu, Y.-M.; Chen, X.-M.; Chang, H.-C.; Mochizuki, K.; Kitagawa, S. *New J. Chem.* **2003**, *27* (5), 779.

(14) Hill, J. A.; Thompson, A. L.; Goodwin, A. L. *J. Am. Chem. Soc.* **2016**, *138* (18), 5886.

(15) Zhang, W.; Cai, Y.; Xiong, R.-G.; Yoshikawa, H.; Awaga, K. *Angew. Chem., Int. Ed.* **2010**, *49* (37), 6608.

(16) Thiele, G.; Messer, D. Z. *Anorg. Allg. Chem.* **1980**, *464* (1), 255.

(17) Schouwink, P.; Ley, M. B.; Tissot, A.; Hagemann, H.; Jensen, T. R.; Smrčok, L.; Černý, R. *Nat. Commun.* **2014**, *5*, 5706.

(18) Bhat, G. A.; Vishnoi, P.; Gupta, S. K.; Murugavel, R. *Inorg. Chem. Commun.* **2015**, *59*, 84.

(19) Maouel, H. A.; Alonzo, V.; Roisnel, T.; Rebbah, H.; Le Fur, E. *Acta Crystallogr., Sect. C: Cryst. Struct. Commun.* **2009**, *65* (7), i36.

(20) Kieslich, G.; Sun, S.; Cheetham, A. K. *Chem. Sci.* **2015**, *6* (6), 3430.

(21) Kieslich, G.; Sun, S.; Cheetham, A. K. *Chem. Sci.* **2014**, *5* (12), 4712.

(22) Wang, B. Q.; Yan, H. B.; Huang, Z. Q.; Zhang, Z. *Acta Crystallogr., Sect. C: Cryst. Struct. Commun.* **2013**, *69* (6), 616.

(23) Maćzka, M.; Ciupa, A.; Gagor, A.; Sieradzki, A.; Pikul, A.; Macalik, B.; Drozd, M. *Inorg. Chem.* **2014**, *53* (10), 5260.

(24) Duyker, S. G.; Hill, J. A.; Howard, C. J.; Goodwin, A. L. *J. Am. Chem. Soc.* **2016**, *138* (35), 11121.

(25) Boström, H. L. B.; Hill, J. A.; Goodwin, A. L. *Phys. Chem. Chem. Phys.* **2016**, *18* (46), 31881.

(26) Kieslich, G.; Kumagai, S.; Butler, K. T.; Okamura, T.; Hendon, C. H.; Sun, S.; Yamashita, M.; Walsh, A.; Cheetham, A. K. *Chem. Commun.* **2015**, *51* (85), 15538.

(27) Howard, C. J.; Zhang, Z. *Acta Crystallogr., Sect. B: Struct. Sci.* **2004**, *60* (2), 249.

(28) Aimi, A.; Mori, D.; Hiraki, K. I.; Takahashi, T.; Shan, Y. J.; Shirako, Y.; Zhou, J.; Inaguma, Y. *Chem. Mater.* **2014**, *26* (8), 2601.

(29) Hafner, J. J. *Comput. Chem.* **2008**, *29* (13), 2044.